European Conference on Computational Fluid Dynamics
ECCOMAS CFD 2006
P. Wesseling, E. Oñate and J. Périaux (Eds)

NUMERICAL SIMULATION OF BUBBLE AND DROPLET DYNAMICS USING PARTITIONED SOLVERS

J. Degroote, J. Vierendeels and E. Dick

Ghent University, Department of Flow, Heat and Combustion Mechanics
St.-Pietersnieuwstraat 41, 9000 Gent, Belgium
e-mail: Joris.Degroote@UGent.be, Jan.Vierendeels@UGent.be and Erik.Dick@UGent.be
web page: http://www.floheacom.ugent.be

Key words: Fluid-Structure Interaction, modal analysis, reduced order model, bubble, droplet

Abstract. *Bubbles and droplets can be simulated as a problem involving Fluid-Structure Interaction (FSI). The interface between the liquid and the gas is then conceived as a zero thickness structure. The position of the interface is determined by the equilibrium between surface tension effects and the pressure jump across the interface. Most techniques frequently used for studying bubble and droplet dynamics, such as Level Set or Volume Of Fluid, use monolithic schemes. The flow on both sides of the interface and the position of the interface are calculated in a single code. Here, a partitioned approach is presented. The flow in the liquid is calculated with a black box commercial code. The position of the interface is calculated with a structural solver, using a reduced order model of the fluid solver to obtain implicit coupling between both solvers. The reduced order model, based on modal analysis, is build up during the coupling iterations of a time step. This model is applied to three axisymmetric problems: an oscillating water droplet in air, an air bubble rising in stagnant mineral oil and the growth and detachment of an air bubble from a vertical needle, submerged in quiescent water.*

1 INTRODUCTION

Bubble and droplet dynamics are studied frequently using different techniques. The dynamics of bubbles and droplets result from the interaction of surface tension on the interface, conceived as a zero thickness structure, with the fluids on both sides of the interface. Techniques such as Level Set[1], Volume Of Fluid[2], Marker And Cell[3], Front Tracking[4], among others, use monolithic schemes. The position of the interface is calculated together with the flow of the fluids on both sides of the interface in a single code.

In this paper, partitioned solvers are used to calculate the interface position and the liquid flow. The solvers are implicitly coupled with an algorithm developed by Vierendeels[5].

In Section 2, the fluid solver and the structural solver are defined. Only axisymmetric problems without mass transfer between the liquid and the gas are considered. Section 3 gives an overview of the coupling algorithm. The application of the model to an oscillating water droplet in air is presented in Section 4. Sections 5 and 6 present an air bubble rising in stagnant mineral oil and the formation of an air bubble at the end of a vertical needle, submerged in quiescent water, respectively.

2 SOLVERS

2.1 Structural solver

As only axisymmetric bubbles and droplets are simulated, the interface is represented by a curve in a meridional plane. This curve is discretised with N nodes. On an interface, equation (1) must be satisfied.

$$(p_1 - p_2 + \sigma\kappa)\boldsymbol{n} = (\mathcal{T}_1 - \mathcal{T}_2) \cdot \boldsymbol{n} + \nabla\sigma \tag{1}$$

A subscript 1 is used to indicate the fluid inside the bubble or droplet, 2 is used for the surrounding fluid. p is the pressure, σ the surface tension coefficient, κ the local surface curvature, $\boldsymbol{n}$ the unit normal to the surface pointing outwards and $\mathcal{T}$ the viscous stress tensor. The pressure jump P across the interface, due to surface tension, is defined in equation (2). This notation allows simultaneous explanation of the solvers and the coupling algorithm for bubbles and droplets.

$$P \equiv p_1 - p_2 \tag{2}$$

If the viscous stresses on the interface and the variation of the surface tension coefficient are neglected, equation (1) simplifies to equation (3).

$$P + \sigma\kappa = 0 \tag{3}$$

Equation (1) contains a normal and tangential condition, equation (3) is scalar. Equation (3) is used here, so surface tension results in only one equation for every interface node.

The surface curvature is defined using the principal radii of curvature R_1 and R_2.

$$\kappa = \frac{1}{R_1} + \frac{1}{R_2} \tag{4}$$

For the calculation of R_1 and R_2 in node i of the interface, a local parametric interpolant of the interface is constructed through node i and two neighbours on each side ($i-2, i-1, i+1, i+2$).

$$x_i(s) = c_0 + c_1 s + c_2 s^2 + c_3 s^3 + c_4 s^4 \tag{5a}$$
$$r_i(s) = d_0 + d_1 s + d_2 s^2 + d_3 s^3 + d_4 s^4 \tag{5b}$$

with x the axial coordinate, r the radial coordinate and s the arc length along the curve representing the interface. The derivatives of expressions (5) evaluated in node i are used to calculate the principal radii of curvature.

$$R_1 = \frac{\left[\left(\frac{\mathrm{d}x}{\mathrm{d}s}\right)^2 + \left(\frac{\mathrm{d}r}{\mathrm{d}s}\right)^2\right]^{\frac{3}{2}}}{\frac{\mathrm{d}x}{\mathrm{d}s}\frac{\mathrm{d}^2r}{\mathrm{d}s^2} - \frac{\mathrm{d}r}{\mathrm{d}s}\frac{\mathrm{d}^2x}{\mathrm{d}s^2}} \tag{6a}$$

$$R_2 = -r\frac{\sqrt{\left(\frac{\mathrm{d}x}{\mathrm{d}s}\right)^2 + \left(\frac{\mathrm{d}r}{\mathrm{d}s}\right)^2}}{\frac{\mathrm{d}x}{\mathrm{d}s}} \tag{6b}$$

Both R_1 and R_2 are negative if the interface is a sphere. On the axis of symmetry, a numerical singularity arises during the calculation of R_2, as both r and $\frac{\mathrm{d}x}{\mathrm{d}s}$ become zero. Using limits and L'Hôpital's rule, it follows that R_2 approaches R_1 as the distance to the axis approaches zero. Thus, on the axis the surface curvature κ is defined as in equation (7).

$$\kappa = \frac{2}{R_1} \tag{7}$$

The left hand side of equation (3) is called $g_{i,1}$.

$$g_{i,1} = P_i + \sigma\kappa_i \tag{8a}$$

The first condition that must be statisfied in every node of the interface is thus given by equation (8b).

$$g_{i,1} = 0 \tag{8b}$$

A second equation in every node keeps the nodes equidistant.

$$\left[(x_i - x_{i-1})^2 + (r_i - r_{i-1})^2\right] - \left[(x_i - x_{i+1})^2 + (r_i - r_{i+1})^2\right] = 0 \tag{9a}$$

The left hand side of equation (9a) is called $g_{i,2}$.

$$g_{i,2} = \left[(x_i - x_{i-1})^2 + (r_i - r_{i-1})^2\right] - \left[(x_i - x_{i+1})^2 + (r_i - r_{i+1})^2\right] \tag{9b}$$

Using this notation, equation (9a) becomes:

$$g_{i,2} = 0 \tag{9c}$$

$g_{i,1}$ and $g_{i,2}$ ($i = 0, \ldots, N-1$) are placed together in a vector $\mathbf{G}$.

$$\mathbf{G} = \begin{bmatrix} g_{0,1}(x_{-2}, r_{-2}, x_{-1}, r_{-1}, x_0, r_0, x_1, r_1, x_2, r_2, P_0) \\ g_{0,2}(x_{-1}, r_{-1}, x_0, r_0, x_1, r_1) \\ g_{1,1}(x_{-1}, r_{-1}, x_0, r_0, x_1, r_1, x_2, r_2, x_3, r_3, P_1) \\ g_{1,2}(x_0, r_0, x_1, r_1, x_2, r_2) \\ \vdots \\ g_{N-1,1}(x_{N-3}, r_{N-3}, x_{N-2}, r_{N-2}, x_{N-1}, r_{N-1}, x_N, r_N, x_{N+1}, r_{N+1}, P_{N-1}) \\ g_{N-1,2}(x_{N-2}, r_{N-2}, x_{N-1}, r_{N-1}, x_N, r_N) \end{bmatrix} \tag{10}$$

Indices outside the range $0, \ldots, N-1$ denote points mirrored around the axis of symmetry. To satisfy equations (8b) and (9c), $\mathbf{G}$ must equal zero.

$$\mathbf{G}(\boldsymbol{X}, \boldsymbol{P}) = 0 \tag{11a}$$

with:

$$\boldsymbol{X} = \begin{bmatrix} x_0 \\ r_0 \\ x_1 \\ r_1 \\ \vdots \\ x_{N-1} \\ r_{N-1} \\ t \end{bmatrix} \quad , \quad \boldsymbol{P} = \begin{bmatrix} P_0 \\ P_1 \\ \vdots \\ P_{N-1} \end{bmatrix} \tag{11b}$$

The reason for including the time t in the position vector $\boldsymbol{X}$ is given later. The code that solves equation (11a) for $\boldsymbol{X}$ is called the *structural solver*.

2.2 Fluid solver

The pressure distributions on the liquid and gas sides of the interface are required to calculate $\boldsymbol{P}$.

The gas pressure is modelled uniform in space, because the pressure variation on the interface is due to inertia ($\rho \frac{\mathrm{D}v}{\mathrm{D}t}$). As the density of a gas is often a thousand times lower than the density of a liquid, the pressure variation on the gas side of the interface can be neglected compared with the variation on the liquid side.

The pressure of a gas surrounding a liquid droplet is modelled constant. The pressure inside a bubble is calculated from the mass, temperature and volume ($\boldsymbol{X}$) of the bubble using the ideal gas law.

A black box commercial code (`Fluent 6.1`) is used to determine the pressure on the liquid side of the interface. The commercial code must be capable to compute the pressure distribution on the liquid side of the interface, given a deformation of this interface. The interface is modelled as a free-slip wall. The position of the interface is not known in advance. The Arbitrary Lagrangian-Eulerian (ALE) description is used for the liquid. The grid nodes close to the interface move along with the interface. A smaller fraction of the interface's displacement is applied as the distance to the interface increases. Large cells are split up, small cells are merged and the skewness of the cells is automatically limited.

`Fluent 6.1` responds on a deformation of the interface with the pressure distribution on the liquid side, which can be converted into $\boldsymbol{P}$ using the uniform gas pressure. The combination of `Fluent` with the conversion program, returning $\boldsymbol{P}$ for given $\boldsymbol{X}$, is called the *fluid solver*. The fluid solver's action is further indicated with $\mathbf{F}$.

$$\boldsymbol{P} = \mathbf{F}(\boldsymbol{X}) \tag{12}$$

3 COUPLING ALGORITHM

Subsequent calls of the structural solver to obtain a new position of the interface and the fluid solver to obtain a new distribution of the pressure jump across the interface, lead to divergence. Explicit coupling of the solvers fails due to the strong interaction of the fluids and the structure. Therefore, the structural problem, equation (11a), has to be solved in an implicit way. To solve equation (11a) for $\boldsymbol{X}$ with implicit calculation of $\boldsymbol{P}$ using Newton's method, the Jacobian of $\mathbf{F}$ is required. As the fluid solver used here is a black box commercial code, the Jacobian is unavailable. Thus, a reduced order model of the fluid solver is constructed using modal analysis. With this reduced order model, an approximation of the Jacobian can be obtained and the pressure jump across the interface can be updated during the Newton iterations.

This coupling procedure is now explained in detail. The values of $\boldsymbol{X}^{n+1}$ and $\boldsymbol{P}^{n+1}$ are calculated, starting from the known values of $\boldsymbol{X}^n$, $\boldsymbol{P}^n$ and $\boldsymbol{V}^n$, with the superscript indicating the time level. $\boldsymbol{V}$ is the vector containing the velocity of the interface nodes.

$$\boldsymbol{V} = \begin{bmatrix} \dot{x}_0 \\ \dot{r}_0 \\ \dot{x}_1 \\ \dot{r}_1 \\ \vdots \\ \dot{x}_{N-1} \\ \dot{r}_{N-1} \end{bmatrix} \tag{13}$$

A subscript k is used to indicate the current coupling iteration.

- **First coupling iteration** $(k = 1)$
  A first guess for the position of the interface on time level $n+1$ is determined using an explicit forward Euler scheme.

  $$\boldsymbol{X}_1^{n+1} = \boldsymbol{X}^n + \boldsymbol{V}^n \Delta t \tag{14}$$

  with Δt the time step. The pressure jump across the interface is obtained from the fluid solver.

  $$\boldsymbol{P}_1^{n+1} = \mathbf{F}^{n+1}\left(\boldsymbol{X}_1^{n+1}\right) \tag{15}$$

  The superscript of the fluid solver indicates that the boundary conditions are updated to time level $n+1$.

- **Second coupling iteration** $(k = 2)$
  The time superscript is now dropped as all variables are at time level $n+1$. $\boldsymbol{X}_2^*$ is calculated explicitly, that is with $\boldsymbol{P} = \boldsymbol{P}_1$, using Newton's method. The Newton iterations are indicated with the subscript j and start from $\boldsymbol{X}_1$.

$$\boldsymbol{X}^*_{2,j+1} = \boldsymbol{X}^*_{2,j} - \left(\frac{\partial \mathbf{G}}{\partial \boldsymbol{X}}\right)^{-1}_{\boldsymbol{X}^*_{2,j}} \cdot \mathbf{G}\left(\boldsymbol{X}^*_{2,j}, \boldsymbol{P}_1\right) \tag{16}$$

As $\boldsymbol{X}^*_2$ is calculated with explicit coupling between the fluid solver and the structural solver, it can differ largely from the exact solution. So, underrelaxation with $\omega = 0.05$ is applied.

$$\boldsymbol{X}_2 = (1-\omega)\boldsymbol{X}_1 + \omega \boldsymbol{X}^*_2 \tag{17}$$

Again, $\boldsymbol{P}$ is calculated using the fluid solver.

$$\boldsymbol{P}_2 = \mathbf{F}(\boldsymbol{X}_2) \tag{18}$$

- **Further coupling iterations** ($k+1$ with $k \geq 2$)
  At the start of coupling iteration $k+1$, k positions of the interface are known, with the corresponding distributions of the pressure jump across the interface. Thus, $k-1$ displacement modes $\boldsymbol{v}_m$ with the corresponding pressure modes $\boldsymbol{w}_m$ are known.

$$\boldsymbol{v}_m = \boldsymbol{X}_k - \boldsymbol{X}_m \tag{19a}$$
$$\boldsymbol{w}_m = \boldsymbol{P}_k - \boldsymbol{P}_m \tag{19b}$$

  with $m = 1, \ldots, k-1$.

  During the solution of equation (11a) for $\boldsymbol{X}$, the position of the interface changes from $\boldsymbol{X}_k$ to $\boldsymbol{X}_{k+1}$. Any displacement $\Delta\boldsymbol{X}_{k+1} = \boldsymbol{X}_{k+1} - \boldsymbol{X}_k$ can be projected on the set of displacement modes. As the dimension of $\boldsymbol{X}$ is bigger than $k-1$, there is a correction term.

$$\Delta\boldsymbol{X}_{k+1} = \sum_{m=1}^{k-1} \alpha_m \boldsymbol{v}_m + \Delta\boldsymbol{X}_{correction} \tag{20a}$$

  The displacement modes are considered to be well chosen, so the correction term is small and can be neglected.

$$\Delta\boldsymbol{X}_{k+1} \approx \sum_{m=1}^{k-1} \alpha_m \boldsymbol{v}_m \tag{20b}$$
$$= \begin{bmatrix}\boldsymbol{v}_1 & \boldsymbol{v}_2 & \ldots & \boldsymbol{v}_{k-1}\end{bmatrix} \begin{bmatrix}\alpha_1 \\ \alpha_2 \\ \vdots \\ \alpha_{k-1}\end{bmatrix} \tag{20c}$$

If the coefficients α_m are known, the change of $\boldsymbol{P}$ corresponding to $\Delta\boldsymbol{X}_{k+1}$ can be calculated.

$$\Delta\boldsymbol{P}_{k+1} = \sum_{m=1}^{k-1} \alpha_m \boldsymbol{w}_m \tag{21a}$$

$$= \begin{bmatrix} \boldsymbol{w}_1 & \boldsymbol{w}_2 & \dots & \boldsymbol{w}_{k-1} \end{bmatrix} \begin{bmatrix} \alpha_1 \\ \alpha_2 \\ \vdots \\ \alpha_{k-1} \end{bmatrix} \tag{21b}$$

The reduced order model for $\boldsymbol{P}$ is given in equation (22).

$$\hat{\boldsymbol{P}}_{k+1} = \boldsymbol{P}_k + \Delta\boldsymbol{P}_{k+1} \tag{22a}$$

$$= \hat{\mathbf{F}}\left(\boldsymbol{X}_{k+1}\right) \tag{22b}$$

To distinguish between distributions of the pressure jump across the interface coming from the reduced order model and distributions from the fluid solver, a hat is used for those from the reduced order model.

As the reduced order model is constructed, it is fully known. So it can be substituted in equation (11a) and its Jacobian can be calculated. Thus, equation (11a) can be solved implicitly using Newton's method, with $\boldsymbol{X}_{k+1,1} = \boldsymbol{X}_k$. After every Newton iteration, $\boldsymbol{P}$ is updated using the reduced order model.

$$\boldsymbol{X}_{k+1,j+1} = \boldsymbol{X}_{k+1,j} - \left(\frac{\partial \mathbf{G}}{\partial \boldsymbol{X}} + \frac{\partial \mathbf{G}}{\partial \boldsymbol{P}} \frac{\partial \hat{\boldsymbol{P}}}{\partial \boldsymbol{X}} \right)^{-1}_{\boldsymbol{X}_{k+1,j}} \cdot \mathbf{G}\left(\boldsymbol{X}_{k+1,j}, \hat{\boldsymbol{P}}_{k+1,j} \right) \tag{23}$$

$$\hat{\boldsymbol{P}}_{k+1,j+1} = \boldsymbol{P}_k + \frac{\partial \hat{\boldsymbol{P}}}{\partial \boldsymbol{X}} \cdot \left(\boldsymbol{X}_{k+1,j+1} - \boldsymbol{X}_k \right) \tag{24}$$

The coefficients α_m and the Jacobian of the reduced order model, used in equations (23) and (24), still have to be defined. As the dimension of $\boldsymbol{X}$ is bigger than $k-1$, equation (20c) shows that the α_m are overdetermined. A least squares technique can be used. Equation (20c) is multiplied with $\boldsymbol{v}_q^{\mathrm{T}}$.

$$\boldsymbol{v}_q^{\mathrm{T}} \Delta\boldsymbol{X}_{k+1} = \begin{bmatrix} \boldsymbol{v}_q^{\mathrm{T}}\boldsymbol{v}_1 & \boldsymbol{v}_q^{\mathrm{T}}\boldsymbol{v}_2 & \dots & \boldsymbol{v}_q^{\mathrm{T}}\boldsymbol{v}_{k-1} \end{bmatrix} \begin{bmatrix} \alpha_1 \\ \alpha_2 \\ \vdots \\ \alpha_{k-1} \end{bmatrix} \tag{25}$$

with $q = 1, \dots, k-1$. These $k-1$ equations are placed together in a matrix.

$$\begin{bmatrix} \boldsymbol{v}_1^{\mathrm{T}} \\ \boldsymbol{v}_2^{\mathrm{T}} \\ \vdots \\ \boldsymbol{v}_{k-1}^{\mathrm{T}} \end{bmatrix} \Delta \boldsymbol{X}_{k+1} = \begin{bmatrix} \boldsymbol{v}_1^{\mathrm{T}}\boldsymbol{v}_1 & \boldsymbol{v}_1^{\mathrm{T}}\boldsymbol{v}_2 & \dots & \boldsymbol{v}_1^{\mathrm{T}}\boldsymbol{v}_{k-1} \\ \boldsymbol{v}_2^{\mathrm{T}}\boldsymbol{v}_1 & \boldsymbol{v}_2^{\mathrm{T}}\boldsymbol{v}_2 & \dots & \boldsymbol{v}_2^{\mathrm{T}}\boldsymbol{v}_{k-1} \\ \vdots & \vdots & \ddots & \vdots \\ \boldsymbol{v}_{k-1}^{\mathrm{T}}\boldsymbol{v}_1 & \boldsymbol{v}_{k-1}^{\mathrm{T}}\boldsymbol{v}_2 & \dots & \boldsymbol{v}_{k-1}^{\mathrm{T}}\boldsymbol{v}_{k-1} \end{bmatrix} \begin{bmatrix} \alpha_1 \\ \alpha_2 \\ \vdots \\ \alpha_{k-1} \end{bmatrix} \tag{26}$$

The coefficients α_m are calculated using matrix inversion. This requires that the displacement modes $\boldsymbol{v}_m$ are linearly independent.

$$\begin{bmatrix} \alpha_1 \\ \alpha_2 \\ \vdots \\ \alpha_{k-1} \end{bmatrix} = \begin{bmatrix} \boldsymbol{v}_1^{\mathrm{T}}\boldsymbol{v}_1 & \boldsymbol{v}_1^{\mathrm{T}}\boldsymbol{v}_2 & \dots & \boldsymbol{v}_1^{\mathrm{T}}\boldsymbol{v}_{k-1} \\ \boldsymbol{v}_2^{\mathrm{T}}\boldsymbol{v}_1 & \boldsymbol{v}_2^{\mathrm{T}}\boldsymbol{v}_2 & \dots & \boldsymbol{v}_2^{\mathrm{T}}\boldsymbol{v}_{k-1} \\ \vdots & \vdots & \ddots & \vdots \\ \boldsymbol{v}_{k-1}^{\mathrm{T}}\boldsymbol{v}_1 & \boldsymbol{v}_{k-1}^{\mathrm{T}}\boldsymbol{v}_2 & \dots & \boldsymbol{v}_{k-1}^{\mathrm{T}}\boldsymbol{v}_{k-1} \end{bmatrix}^{-1} \begin{bmatrix} \boldsymbol{v}_1^{\mathrm{T}} \\ \boldsymbol{v}_2^{\mathrm{T}} \\ \vdots \\ \boldsymbol{v}_{k-1}^{\mathrm{T}} \end{bmatrix} \Delta \boldsymbol{X}_{k+1} \tag{27}$$

The Jacobian of the reduced order model is given by equation (28).

$$\frac{\partial \hat{\boldsymbol{P}}}{\partial \boldsymbol{X}} = \frac{\partial \Delta \boldsymbol{P}}{\partial \boldsymbol{X}} \tag{28a}$$

$$= \begin{bmatrix} \boldsymbol{w}_1 & \boldsymbol{w}_2 & \dots & \boldsymbol{w}_m \end{bmatrix} \frac{\partial}{\partial \boldsymbol{X}} \begin{bmatrix} \alpha_1 \\ \alpha_2 \\ \vdots \\ \alpha_{k-1} \end{bmatrix} \tag{28b}$$

$$= \begin{bmatrix} \boldsymbol{w}_1 & \boldsymbol{w}_2 & \dots & \boldsymbol{w}_m \end{bmatrix} \begin{bmatrix} \boldsymbol{v}_1^{\mathrm{T}}\boldsymbol{v}_1 & \dots & \boldsymbol{v}_1^{\mathrm{T}}\boldsymbol{v}_{k-1} \\ \vdots & \ddots & \vdots \\ \boldsymbol{v}_{k-1}^{\mathrm{T}}\boldsymbol{v}_1 & \dots & \boldsymbol{v}_{k-1}^{\mathrm{T}}\boldsymbol{v}_{k-1} \end{bmatrix}^{-1} \begin{bmatrix} \boldsymbol{v}_1^{\mathrm{T}} \\ \vdots \\ \boldsymbol{v}_{k-1}^{\mathrm{T}} \end{bmatrix} \tag{28c}$$

When the Newton iterations have converged, the fluid solver is used to obtain $\boldsymbol{P}_{k+1}$.

$$\boldsymbol{P}_{k+1} = \mathbf{F}\left(\boldsymbol{X}_{k+1}\right) \tag{29}$$

Using the distribution of the pressure jump from the fluid solver, the residual is calculated.

$$\mathbf{G}\left(\boldsymbol{X}_{k+1}, \boldsymbol{P}_{k+1}\right) \tag{30}$$

The root-mean-square of expression (30) should decrease three or four orders of magnitude to obtain convergence of the time step. If the residual has decreased enough, the time step has converged. Otherwise, another coupling iteration has to be performed.

If the time step is sufficiently small, the modes of the previous time step are still relevant. They are reused to make a better reduced order model and thus to reduce the required number of coupling iterations. This is the reason for including t in $\boldsymbol{X}$.

4 OSCILLATING DROPLET

Using the implicitly coupled partitioned solvers, the oscillation of a water droplet in air is simulated. The unstructured grid used to calculate the water flow is shown in Figure 1. The horizontal and vertical edges of the grid are the axes of the coordinate system. The

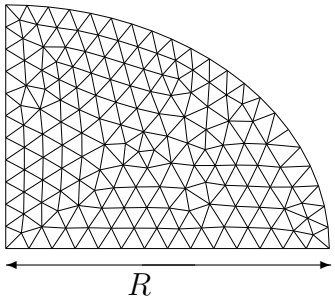

Figure 1: The unstructured grid used to calculate the flow in the water.

problem is considered to be axisymmetric around the horizontal axis, but also symmetric around the vertical axis. Gravity is neglected. The initial situation is an ellipsoid droplet of water at rest. The distance between the origin and the intersection of the horizontal axis with the interface is denoted as R. The oscillation amplitude reduces due to viscosity and the droplet evolves to a sphere with equilibrium radius R_0.

The physical properties of water (subscript 1) and the water-air interface used for the simulations are given in equation (31).

$$\begin{cases} \rho_1 &= 998.2\,\mathrm{kg/m^3} \\ \mu_1 &= 0.001003\,\mathrm{Pa\,s} \\ \sigma &= 0.070\,\mathrm{N/m} \end{cases} \tag{31}$$

4.1 Small amplitude oscillation

The angular frequency of the small amplitude oscillation can be compared with the linear, irrotational approximation for low viscosity fluids by Lamb[6], who splits the droplet oscillation in an infinite series of spherical harmonics. The angular frequency of the l^{th} mode of an oscillating liquid droplet is given by equation (32a).

$$\hat{\omega}_l = \omega_l \sqrt{1 - (\omega_l \tau_l)^{-2}} \tag{32a}$$

with:

$$\omega_l{}^2 = \frac{\sigma}{\rho {R_0}^3} l(l-1)(l+2) \tag{32b}$$

$$\tau_l = \frac{\rho {R_0}^2}{\mu(l-1)(2l+1)} \tag{32c}$$

Figure 2 shows R/R_0 as a function of time for a droplet with $R_0 = 1.48\,\text{mm}$ and initial deformation $R = 1.07R_0$. 20 nodes on the interface and time steps of 0.35 ms are used. The oscillation period is 15.05 ms, resulting in an angular frequency of $\omega = 417.49\,\text{rad/s}$. With the parameters stated in equation (31), equation (32a) yields $\hat{\omega}_2 = 418.26\,\text{rad/s}$.

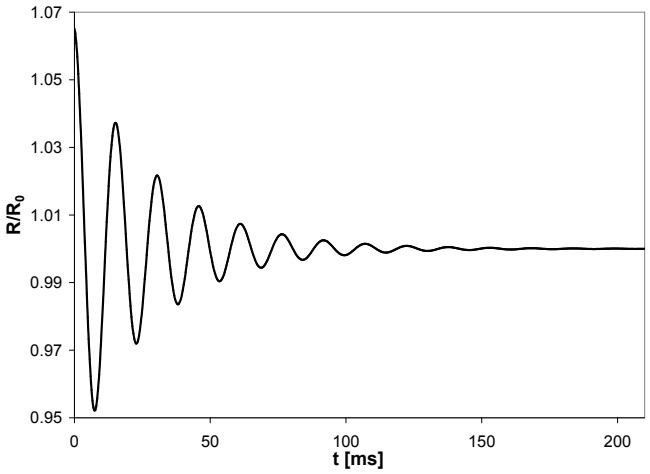

Figure 2: Small amplitude oscillation of a water droplet in air, with $R_0 = 1.48\,\text{mm}$ and initial deformation $R = 1.07R_0$.

4.2 Large amplitude oscillation

Large amplitude oscillation of a droplet can also be studied using the model. One oscillation period of a droplet with $R_0 = 1.65\,\text{mm}$ and initial deformation $R = 1.21R_0$ is simulated in 54 time steps with 30 nodes on the interface. The velocity vectors are shown in Figure 3. The number of new modes required each time step of the first oscillation period is given in Figure 4(a), with an average of 4.46. The modes of the previous time step are used to make a better reduced order model. If the modes of the two previous time steps are used, the algorithm does not work properly, especially not when the direction of the motion reverses. Modes of the previous time steps are no longer relevant in that situation and convergence can not be obtained. The convergence behaviour of the fastest and slowest converging time step is shown in Figure 4(b).

For the large amplitude oscillation, a grid dependence study has been done with 10, 20, 40, 80 and 160 nodes on the interface. Figure 5 shows R as a function of time for the different numbers of nodes, together with a Richardson extrapolation using the data from the simulations with 40, 80 and 160 nodes. The minimum and maximum of R during the first period of the oscillation are studied more in detail in Table 1. The *Error* is the relative difference with the Richardson extrapolation. From the value of α, which is close to unity, it can be seen that the algorithm is first-order accurate.

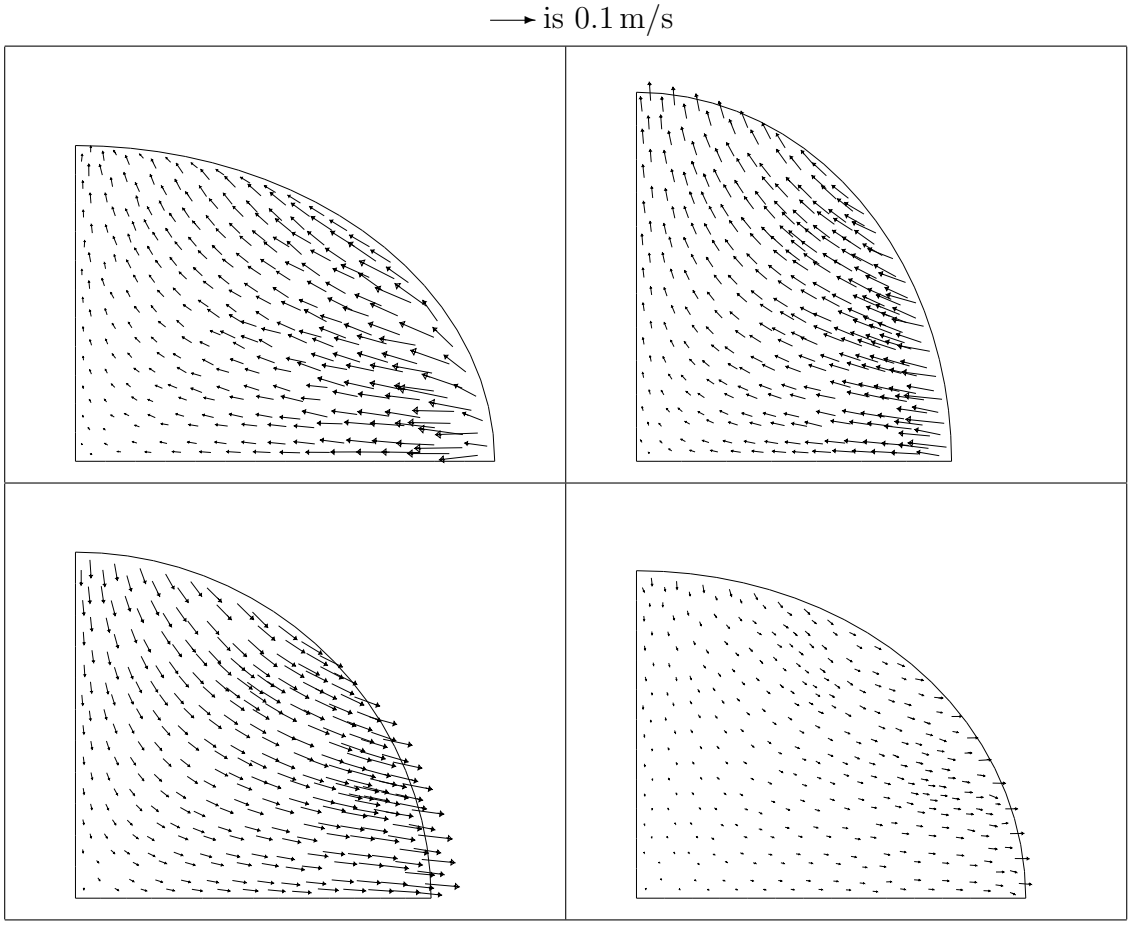

Figure 3: Velocity vectors of the large amplitude oscillation with 30 nodes on the interface after 0.35 ms, 7 ms, 14 ms and 17.5 ms.

Number of nodes	Minimum [mm]	Error [%]	Maximum [mm]	Error [%]
10	1.46	9.04	1.77	9.87
20	1.42	6.28	1.86	5.64
40	1.39	3.45	1.91	2.97
80	1.36	1.89	1.94	1.35
160	1.35	1.04	1.95	0.71
Extrapolation	1.34		1.97	
α	0.862		0.928	

Table 1: Richardson extrapolation of the minimum and maximum of R during the first oscillation period of the large amplitude oscillation.

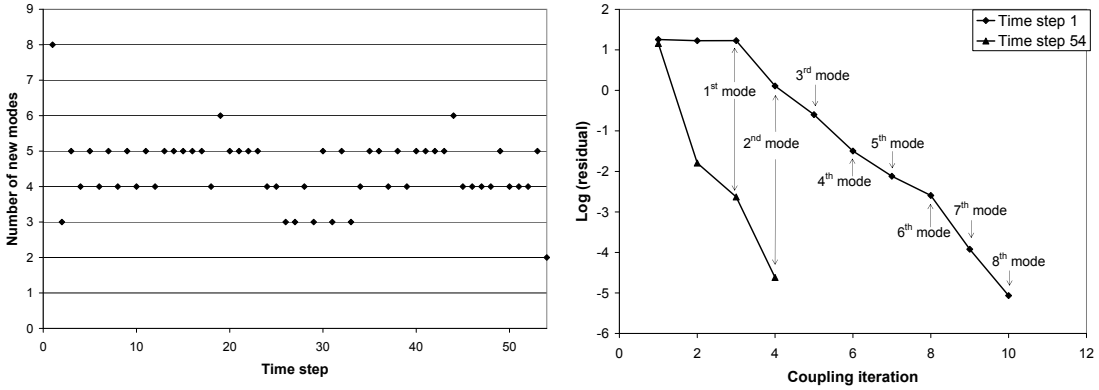

(a) (b)

Figure 4: (a) The number of new modes required each time step of the first period of the large amplitude oscillation with 30 nodes on the interface and (b) the convergence behaviour of the coupling iterations for time step 1 (8 new modes) and 54 (2 new modes).

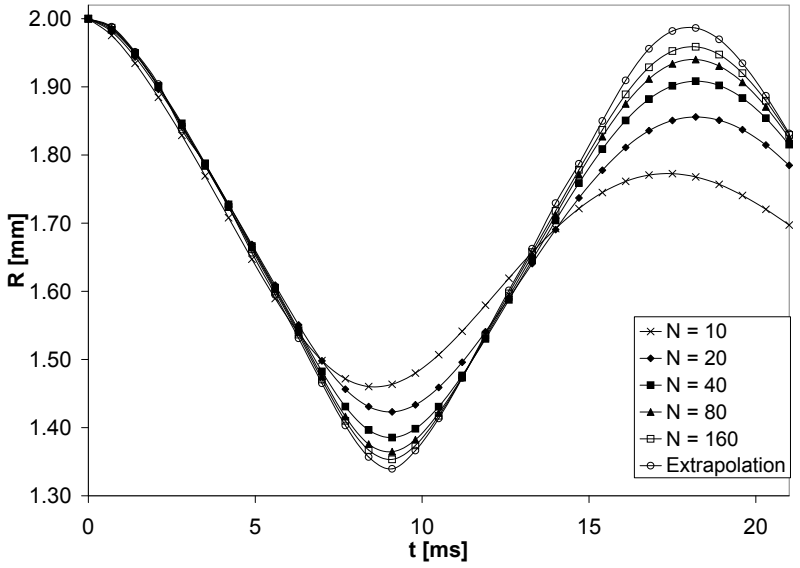

Figure 5: R as a function of time for the large amplitude oscillation using 10, 20, 40, 80 and 160 nodes on the interface, together with a Richardson extrapolation.

5 RISING BUBBLE

The second application is an air bubble rising in stagnant mineral oil, due to gravity. This is simulated using a grid in a moving reference frame. There are two possibilities to determine the velocity of the reference frame. It can be held fixed during the time step, allowing all the nodes on the interface to move. After the time step the velocity of the reference frame is increased by the amount the bubble center has risen in the relative frame divided by the time step. This way, the bubble only rises a little, minimizing grid distortion. The velocity of the reference frame can also be a variable during the coupling iterations of the time step. The top of the bubble is then fixed. Equation (3) in the fixed node is satisfied by changing the velocity of the reference frame. The axial coordinate of the fixed node is substituted in the displacement modes by the reference frame velocity. The former method results in faster convergence and is more robust than the latter.

It should be mentionned that most authors neither neglect viscous forces on the interface nor the flow within the bubble, when studying a rising bubble. As recommended by Harmaty[7], we chose the size of the liquid domain equal to ten times the bubble diameter in all directions.

Bubble A from Table I in Hnat and Buckmaster[8] has been simulated with 52 nodes on the interface and time steps of 0.0025 s. This is a spherical cap bubble of 0.94 ml without skirts, rising in mineral oil with the properties given in equation (33).

$$\begin{cases} \rho_2 &= 875.5\,\mathrm{kg/m^3} \\ \mu_2 &= 0.118\,\mathrm{Pa\,s} \\ \sigma &= 0.0322\,\mathrm{N/m} \end{cases} \tag{33}$$

The build up of the velocity in the bubble's center of mass is shown in Figure 6(a). The shape of the bubble after 0.5 s is given in Figure 6(b). The terminal velocity is 0.2437 m/s, which differs 12 % from the experimental value. The shape agrees reasonably well with the experiment.

6 BUBBLE GROWTH AND DETACHMENT FROM A VERTICAL NEEDLE

The third application of the model is the growth and detachment of an air bubble from a vertical needle with inner radius a, submerged in quiescent water. A specific case already studied experimentally by Longuet-Higgins et al.[9] and numerically by Oğuz et al.[10], has been simulated.

The air mass flow rate $\dot{m}$ through the needle is modelled as done by Oğuz et al.[10].

$$\dot{m} = \frac{\pi}{16}\frac{a^4}{l\mu_1}\frac{{p_C}^2 - {p_1}^2}{\mathcal{R}T} \tag{34}$$

with p_C the pressure in the device delivering the mass flow, $\mathcal{R}$ the gas constant of air and T the temperature which is modelled constant. p_1 and μ_1 are the pressure and dynamic

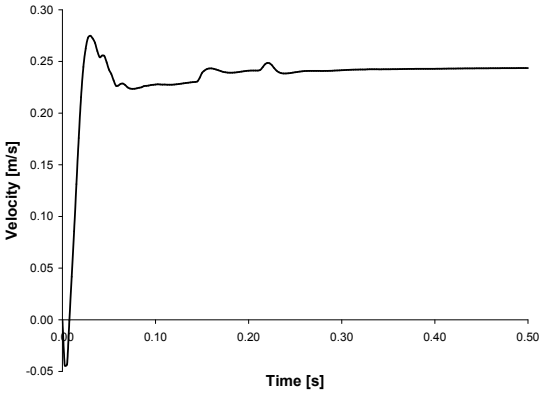

(a)

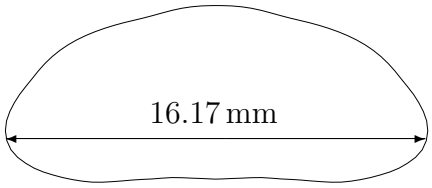

(b)

Figure 6: Simulation of bubble A in Table I from Hnat and Buckmaster[8]. (a) Rise velocity as a function of time and (b) bubble shape after 0.5 s.

viscosity inside the bubble, so the values for air. l is the effective length of the needle. Constrictions are converted into an equivalent needle length.

Equation (34) is integrated implicitly in time, to avoid explicit time step restrictions.

$$m^{n+1} = m^n + \frac{\pi}{16}\frac{a^4}{l\mu_1}\frac{{p_C}^2 - {p_1^{n+1}}^2}{\mathcal{R}T} \tag{35}$$

The air pressure is calculated using the ideal gas law.

$$p_1^{n+1} = \frac{m^{n+1}\mathcal{R}T}{V^{n+1}} \tag{36}$$

with V the volume of the bubble, calculated from the position of the interface nodes. Equations (35) and (36) are a set of two equations, resulting in a quadratic equation for m^{n+1}. The physically correct solution for m^{n+1} is selected and then substituted in equation (36) to obtain p_1^{n+1}

The bubble starts as half a sphere at the end of the needle. In this situation the radii of curvature are at their lowest value, so the air pressure p_1 in the bubble is maximal.

$$p_1 = p_\infty + \frac{2\sigma}{a} \tag{37}$$

with p_∞ the stagnation pressure at the needle's tip on the water side of the interface. This situation can only be reached if $p_C > p_\infty + 2\sigma/a$.

For this simulation the parameters stated in (38) are used, resulting in a volumetric growth rate around $200\,\mathrm{mm}^3/\mathrm{s}$.

$$\begin{cases} p_\infty & = 1\,\text{bar} \\ p_C & = 1.00073\,\text{bar} \\ \sigma & = 0.070\,\text{N/m} \\ \mu_1 & = 1.81 \cdot 10^{-5}\,\text{Pa s} \\ \mu_2 & = 0.001003\,\text{Pa s} \\ \rho_2 & = 998.2\,\text{kg/m}^3 \\ l & = 128\,\text{m} \end{cases} \tag{38}$$

The velocity vectors in the water around the bubble are shown in Figure 7. This simulation is done with 31 nodes on the bubble edge before detachment and 32 nodes afterwards. The unstructured grid in the water consists of about 4000 cells. The point where the interface thouches the needle's top is fixed. Good agreement is found between this Figure and Figure 4 in Oğuz et al.[10].

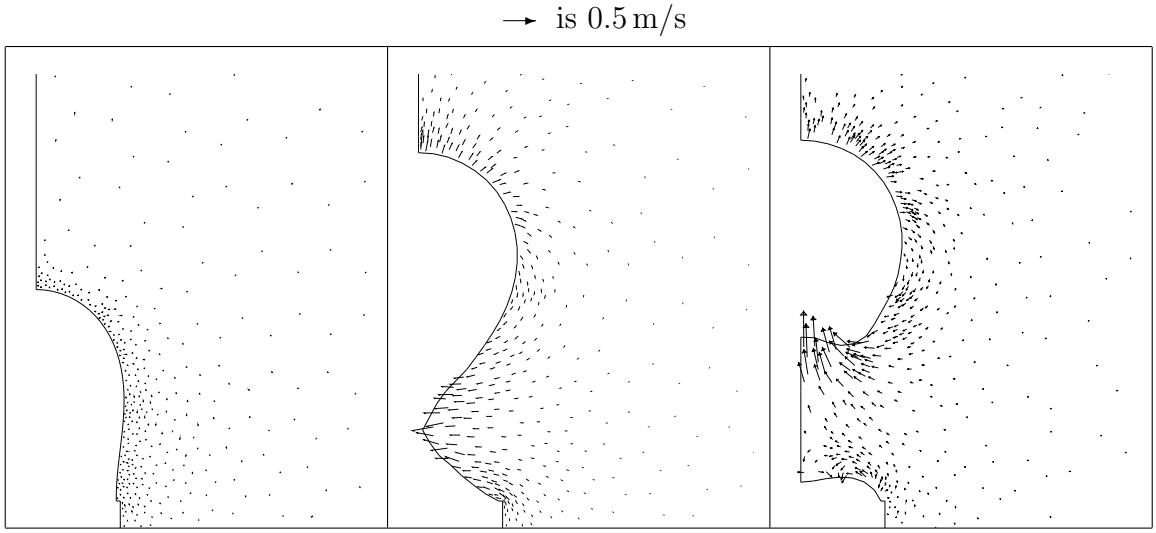

Figure 7: Velocity vectors of an air bubble detaching from a vertical needle at -97.0 ms, at detachment ($t = 0$ ms) and 2.7 ms afterwards.

Figure 8(a) shows the number of new modes needed to drop the residual by four orders of magnitude during each time step of bubble growth, with an average of 4.32. At time step 300, Δt is reduced from 2 ms to 0.1 ms. 6 out of 410 time steps use more than 10 new modes. Figure 8(b) shows the convergence behaviour of the coupling iterations for the fastest and slowest converging time step.

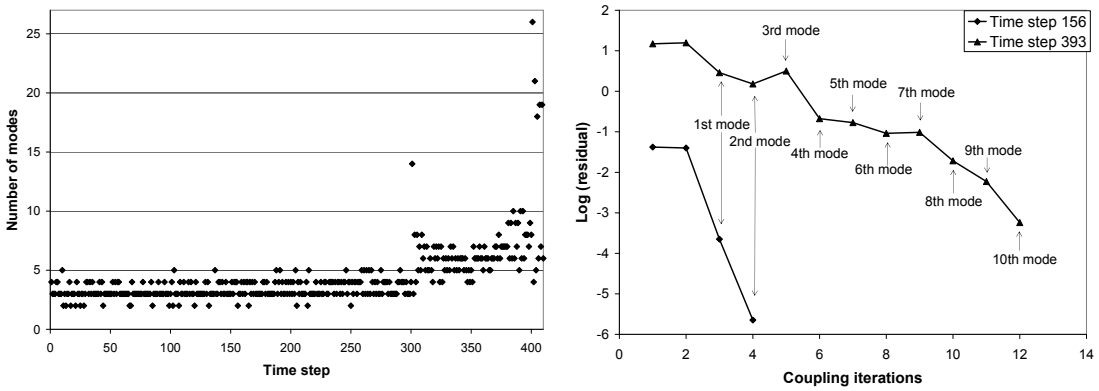

(a) (b)

Figure 8: (a) The number of new modes required each time step during bubble growth with 31 nodes on the interface and (b) the convergence behaviour of the coupling iterations for time step 156 (2 new modes) and 393 (10 new modes).

7 CONCLUSIONS

The ALE description allows a very accurate representation of the interface of bubbles and droplets. The position of the interface is calculated with a structural solver using a reduced order model for the black box fluid solver. The reduced order model allows efficient implicit coupling of the partitioned solvers. The model has succesfully been applied to an axisymmetric water droplet oscillating in air and an air bubble growing and detaching from a vertical needle, submerged in quiescent water. For an air bubble rising in stagnant mineral oil, less agreement with experiments is obtained.

REFERENCES

[1] M. Sussman, E. Fatemi, P. Smereka and S. Osher. An improved level set method for incompressible two-phase flows. *Computers & Fluids*, **27**, 663–680, (1998).

[2] B. Lafaurie, D. Nardone, R. Scardovelli, S. Zaleski and G. Zanetti. Modelling merging and fragmentation in multiphase flows with surfer. *Journal of Computational Physics*, **113**, 134–147, (1994).

[3] M. Tomé and S. McKee. Gensmac: A computational marker and cell method for free surface flows in general domains. *Journal of Computational Physics*, **110**, 171–186, (1994).

[4] G. Ryskin and L. Leal. Numerical solution of free-boundary problems in fluid mechanics. Part 2. Bouyancy-driven motion of a gas bubble through a quiescent liquid. *Journal of Fluid Mechanics*, **148**, 19–35, (1984).

[5] J. Vierendeels. Implicit coupling of partitioned fluid-structure interaction solvers using a reduced order model. In *Proc. of the 35th AIAA Fluid Dynamics Conference and Exhibit*, vol. AIAA-2005-5135. Toronto, Ontario, Canada, (2005).

[6] H. Lamb. *Hydrodynamics*. Cambridge University Press, 6 ed., 1932.

[7] T.Z. Harmathy. Velocity of large drops and bubbles in media of infinite or restricted extent. *American Institute of Chemical Engineers Journal*, **6**, 281–288, (1960).

[8] J.G. Hnat and J.D. Buckmaster. Spherical cap bubbles and skirt formation. *The Physics of Fluids*, **19**, 182–194, (1976).

[9] M. Longuet-Higgins, B. Kerman and K. Lunde. The release of air bubbles from an underwater nozzle. *Journal of Fluid Mechanics*, **230**, 365–390, (1991).

[10] H. Oğuz and A. Prosperetti. Dynamics of bubble growth and detachment from a needle. *Journal of Fluid Mechanics*, **257**, 111–145, (1993).